Strong marine-derived nitrous acid (HONO) production observed in the coastal atmosphere of northern China

Juan Yang [a], Hengqing Shen [a],[**], Ming-Zhi Guo [b],[***], Min Zhao [a], Ying Jiang [a], Tianshu Chen [a], Yuhong Liu [a], Hongyong Li [a], Yujiao Zhu [a], He Meng [c], Wenxing Wang [a], Likun Xue [a],[d],[e],[*]

[a] Environment Research Institute, Shandong University, Qingdao, Shandong, 266237, China
[b] College of Mechanics and Materials, Hohai University, Nanjing, Jiangsu, 210098, China
[c] Qingdao Eco-environment Monitoring Center of Shandong Province, Qingdao, Shandong, 266003, China
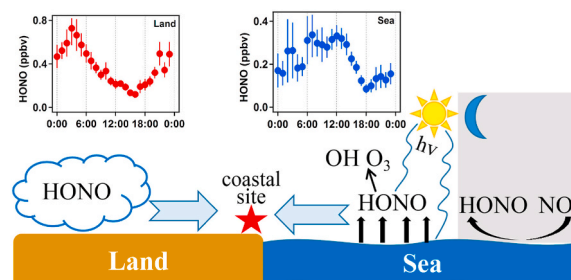[d] Collaborative Innovation Center for Climate Change, Nanjing, Jiangsu, 210023, China
[e] Ji'nan Eco-Environmental Monitoring Center of Shandong Province, Ji'nan, Shandong, 250000, China

HIGHLIGHTS

- The marine-derived HONO in the coastal atmosphere was confirmed.
- High HONO production was observed in both the day and night of maritime air masses.
- The marine-derived HONO contributed significantly to the formation of OH and O_3.

GRAPHICAL ABSTRACT

ARTICLE INFO

ABSTRACT

Despite its important roles in the formation of hydroxyl radical (OH) and ozone (O_3), the characteristics and sources of nitrous acid (HONO) in the marine atmosphere are still poorly understood. In this study, the HONO production in maritime air masses was explored based on a field observation conducted at a coastal site in Qingdao, China in the summer of 2019. The "sea case" and the "land case" were carefully distinguished according to wind direction and backward air mass trajectory. About four times larger nocturnal NO_2-to-HONO conversion rate and ~60% larger daytime P_{other} (production rate of HONO other than gas-phase OH + NO reaction) at noon were observed in the "sea case" compared to the "land case" (0.045 ± 0.014 h^{-1} versus 0.012 ± 0.007 h^{-1}, and 1.83 ± 0.02 ppbv h^{-1} versus 1.14 ± 0.07 ppbv h^{-1}, respectively). Correlation analysis implied that heterogeneous conversion of NO_2 and photolysis of nitrogen-containing compounds were potentially important sources of marine atmospheric HONO in the nocturnal and daytime, respectively, though alkaline oceans are previously considered as sinks of HONO. The impacts of these marine-derived HONO on OH and O_3 were comparable to or larger than that of the "land case". These results suggest that strong marine-derived

HONO production may have been overlooked previously, and more studies are required to explore its detailed formation mechanisms in the marine atmosphere.

1. Introduction

Nitrous acid (HONO) plays an important role in the atmospheric oxidation capacity, and contributes significantly to the production of both hydroxyl radical (OH) and ozone (O_3) (Cui et al., 2019; Su et al., 2008b; Xue et al., 2014). Massive field observations have been conducted in the past several decades to explore its characteristics and sources in urban (Amoroso et al., 2007; Bernard et al., 2015; Huang et al., 2017; Lee et al., 2016; Li et al., 2018; Spataro et al., 2013; Zhang et al., 2018), suburban (Alicke et al., 2002; Michoud et al., 2014; Tong et al., 2015; Yang et al., 2014), rural (Li et al., 2012; Su et al., 2008b; Tsai et al., 2018; Gu et al., 2020), forest (Kleffmann et al., 2005; Ren et al., 2010; Zhang et al., 2009, 2012), mountain areas (Acker et al., 2006; Zhou et al., 2007), and even polar regions (Villena et al., 2011; Zhou et al., 2001). Various sources have been proposed to account for the concentration underestimation when only considering the gas-phase reaction of OH and NO, including direct emissions (vehicle exhaust, ship emissions, biomass burning, and soil) (Kurtenbach et al., 2001; Nie et al., 2015; Su et al., 2011; VandenBoer et al., 2014; Sun et al., 2020), and heterogeneous conversion of NO_2 on various surfaces of aerosols, ground, and vegetation (Spataro and Ianniello, 2014).

Oceans cover more than 70 percent of the Earth's surface, while field measurements about marine atmospheric HONO are very limited. About 10 parts per trillion by volume of HONO have been observed in the marine atmosphere with a slight influence from coastal emissions. The photolysis of particulate nitrate was proposed to be a substantial source (Ye et al., 2016), but its relative contribution is still under debate. The relatively high nocturnal NO_2-to-HONO conversion rates (Zha et al., 2014) and persistently high HONO concentrations during the daytime (Meusel et al., 2016) have been observed (potentially affected by maritime air masses). These differences are usually attributed to non-marine factors, such as the emission of microbial communities on soil surfaces or photolysis of particulate nitrate (Benedict et al., 2017; Meusel et al., 2016; Ye et al., 2016), and alkaline oceans are previously considered as an efficient sink of HONO. However, these continuously observed differences of HONO production in the marine atmosphere indicated that there might be some marine-derived HONO sources that have been overlooked so far (Cui et al., 2019; Wen et al., 2019). Overall, there is little knowledge about thecharacteristics, formation mechanisms, and environmental consequences of HONO in the marine atmosphere, and no research to fully explore the potential marine-derived HONO sources (Cui et al., 2019; Wen et al., 2019; Wojtal et al., 2011).

The coastal area is an ideal place to study the different characteristics of HONO between marine and continental atmosphere. In this study, we conducted a field observation of HONO at a coastal site of Qingdao, northern China, from July 1 to August 25, 2019, and analyzed the characteristics, nocturnal NO_2-to-HONO conversion, and the 'missing' daytime HONO source in the maritime air masses. Strong marine-derived HONO production was confirmed, which significantly perturb the atmospheric oxidation and O_3 formation under the circulation of sea-land breezes, and calls on further studies to pin down its formation mechanisms in the maritime air.

2. Methods

2.1. Study site

The atmospheric HONO was measured on a third-floor building (10 m above the ground) in Qingdao campus of Shandong University ($36.37°$ N, $120.69°$ E), a coastal site in the northeast of Qingdao, China, from July 1 to August 25, 2019. This coastal site is a relatively clean area with over 40 km away from Qingdao downtown, and separated by Mount Lao of 1130 m above sea level (Fig. 1). The measurement site is about 500 m from the nearest sea, and has a more than $150°$ sea view with the open sea extended out from the northeast to the south. This site is less affected by anthropogenic emissions because there are no significant industrial or vehicle sources of pollutant emissions between the measurement site and the sea, and the ship emissions are also minor. Thus, this study site is representative of the rural coastal atmosphere.

2.2. Measurement techniques

HONO was measured by the long-path absorption photometer (*LOPAP, Model 03, QUMA, Germany*), which has been widely used in the field measurements of HONO, and the details could be found in our previous studies (Li et al., 2018; Wen et al., 2019). Ambient air was sampled at a flow rate of 1 L min^{-1} into an external sampling unit under a constant temperature of 20 °C. Gaseous HONO was converted into an azodye in the instrument, and then was detected photo-metrically in a long-path absorption tube. The LOPAP device was conceived as a 2-channel system to correct for potential interferences. In channel 1, HONO and interfering gases were measured, but in channel 2 only interfering nitrogen compounds were measured. The HONO concentration was then determined by the difference between channel 1 and 2. The calibrations of "zero air" (high purity nitrogen of 99.999%) and nitrite standard solution were performed every 11 h and every four days, respectively. The detection limit of HONO was 0.2 pptv with a time resolution of 30 s.

The ambient concentrations of O_3, NO_x, SO_2, and CO were measured by widely-used commercial analyzers of Model 49i, Model 42i, Model 43i, and Model 48i (*Thermo Scientific, USA*), respectively, with detection limits of 0.5 ppbv, 0.05 ppbv, 0.12 ppbv, and 40 ppbv, respectively. Ambient volatile organic compounds (VOCs), including 46 kinds of C_2–C_{12} non-methane hydrocarbons (NMHCs) and 13 kinds of oxygenated volatile organic compounds (OVOCs), were measured by multi-column gas chromatography (GC) coupled with flame ionization detection (FID) and mass spectrometer detection (MSD) (*GC-MS, Trace1300 + ISQ, Thermo Scientific, USA*). The detection limits of the measured VOCs were about 0.1 ppbv, and the measurement precision was about 5%. More detailed information of these instruments could be found in our previous studies (Wang et al., 2012; Xue et al., 2014). The meteorological parameters (wind speed, wind direction, relative humidity, and temperature) and concentrations of $PM_{2.5}$ were obtained from an ambient air quality monitoring station of Qingdao, about 2 km away from the sampling site.

2.3. Definition of "sea case" and "land case"

The "sea case" and the "land case" were carefully distinguished by wind direction and backward air mass trajectory. The "sea/land case" was defined as time periods with wind directions of $30°$–$180°$/$0°$–$30°$ and $180°$–$360°$ (clockwise) and no sudden change within 1 h, and less than 1-h traveling time over the land/sea of its 6-h backward air mass trajectory. The definition was described in detail in Table S1. Time periods that fail to meet the two criteria of wind direction and back trajectory were discarded. The backward trajectories starting at 50-m arrival height were calculated by the Hybrid Single Particle Lagrangian Integrated Trajectory (HYSPLIT) model using the meteorological field from Global Data Assimilation System (GDAS). Finally, 81 "sea case" and 30 "land case" were selected, and time periods of these cases are provided in Table S2. The overall results and one specific case were also provided in Fig. S1 and Fig. S2, respectively.

2.4. Chemical box model

The zero-dimensional Observation-Based Model for investigating Atmospheric Oxidative Capacity and Photochemistry (OBM-AOCP) built on the Master Chemical Mechanism (MCM v3.3.1) was used to elucidate the impacts of HONO on OH and O_3 production (Xue et al., 2016). The model was constrained by measured VOCs, CO, NO, NO_2, SO_2, HONO, O_3, and physical parameters (i.e., water vapor concentration and temperature), and pre-run for two days with the constraints of the entire measured data in both the "sea case" and the "land case". The time step of the model was set to 5 min. Two simulations with and without the constraints of measured HONO were designed to explore the contribution of marine-derived HONO to OH and O_3 production.

3. Results and discussion

3.1. Concentration levels and diurnal variations

The average concentration (±standard deviations, SD) of HONO was 0.315 ± 0.290 ppbv during the study, which was lower than that measured in urban areas (Bernard et al., 2015; Li et al., 2018; Qin et al., 2009; Spataro et al., 2013; Zhang et al., 2018), but was comparable to or higher than that measured at other coastal sites (Cui et al., 2019; Meusel et al., 2016; Wen et al., 2019; Gu et al., 2020). The diurnal variations of HONO and HONO/NO_2 were provided in Fig. S3. The average value of HONO/NO_2 peaked at daytime, and was up to 0.13 at noon, which was different from that measured in the continental atmosphere (Qin et al., 2009; Wang et al., 2013; Li et al., 2018), usually with higher ratios at night. The daytime HONO concentration was also relatively high, with an average daytime value of 0.3 ppbv.

Fig. 2 shows the diurnal variations of HONO, HONO/NO_2, and other measured parameters in the "sea case" and the "land case", and their average values are summarized in Table S3. The concentrations of pollutants were relatively low in both the "sea case" and the "land case" compared with those of the polluted urban areas (Huang et al., 2017; Qin et al., 2009; Zhang et al., 2018), indicating that this measurement site is a relatively clean area. However, there remains a clear difference between the "sea case" and the "land case". The concentrations of CO and SO_2 in the "land case" were much higher than that in the "sea case", 2.3 (479 ppbv versus 203 ppbv) and 1.6 (2.4 ppbv versus 1.5 ppbv) times higher, respectively, and relative humidity (RH) was significantly lower

in the "land case" (Fig. 2h). These are in line with the expectations of maritime air masses, which are usually cleaner and contain more water vapor, indicating that the above-mentioned classification method of the "sea case" and the "land case" is reasonable and maritime air masses were less affected by direct emissions of ships, etc. HONO concentration of the "land case" is higher than that of the "sea case" (0.382 ± 0.291 versus 0.216 ± 0.207, $p < 0.01$), especially in the nighttime (0.472 ppbv versus 0.175 ppbv, $p < 0.01$). This was consistent with the significantly higher nighttime NO_2 concentration of the "land case" (8.03 ppbv versus 3.69 ppbv, $p < 0.01$).

However, the diurnal variations of HONO are totally different between the "sea case" and the "land case". In the "land case", HONO accumulated in the nighttime, and continuously decreased during the entire daytime, which was consistent with the pattern observed in previous continental environments (Huang et al., 2017; Nie et al., 2015; Wen et al., 2019; Qin et al., 2009; Zhang et al., 2018; Michoud et al., 2014). In comparison, the HONO concentration of the "sea case" maintained a relatively high level during the daytime, even higher than that of the "land case" at noon. This difference was more obvious for the ratio of HONO/NO_2. Such a ratio in the "sea case" was over two times higher than that in the "land case" at noon (0.160 versus 0.073). More interestingly, the phenomenon of a persistently high HONO concentration during the daytime was also found in some other marine or coastal areas (Cui et al., 2019; Meusel et al., 2016; Wen et al., 2019), indicating that there may be some neglected HONO sources in the marine atmosphere that are different from the continental environments. In section 3.2 and 3.3, we discussed the nocturnal and daytime production of HONO in marine air masses through the NO_2-to-HONO conversion rate and the production rate of unknown HONO source, respectively.

3.2. High nocturnal NO_2-to-HONO conversion rate

The nighttime HONO is proposed to be mainly formed from the heterogeneous conversion of NO_2 on various wet surfaces (Finlayson-Pitts et al., 2003). The observed NO_2-to-HONO conversion rate (C_{HONO}, Equation (1)) under stable meteorological conditions was often used to determine the strength of this source (Alicke et al., 2002; Su et al., 2008a). To explore the impacts of maritime air masses on the nocturnal HONO production, here, C_{HONO} was calculated. The cases used for this calculation were selected from the "sea case" and the "land case" mentioned in Section 2.3 according to the following five criteria:
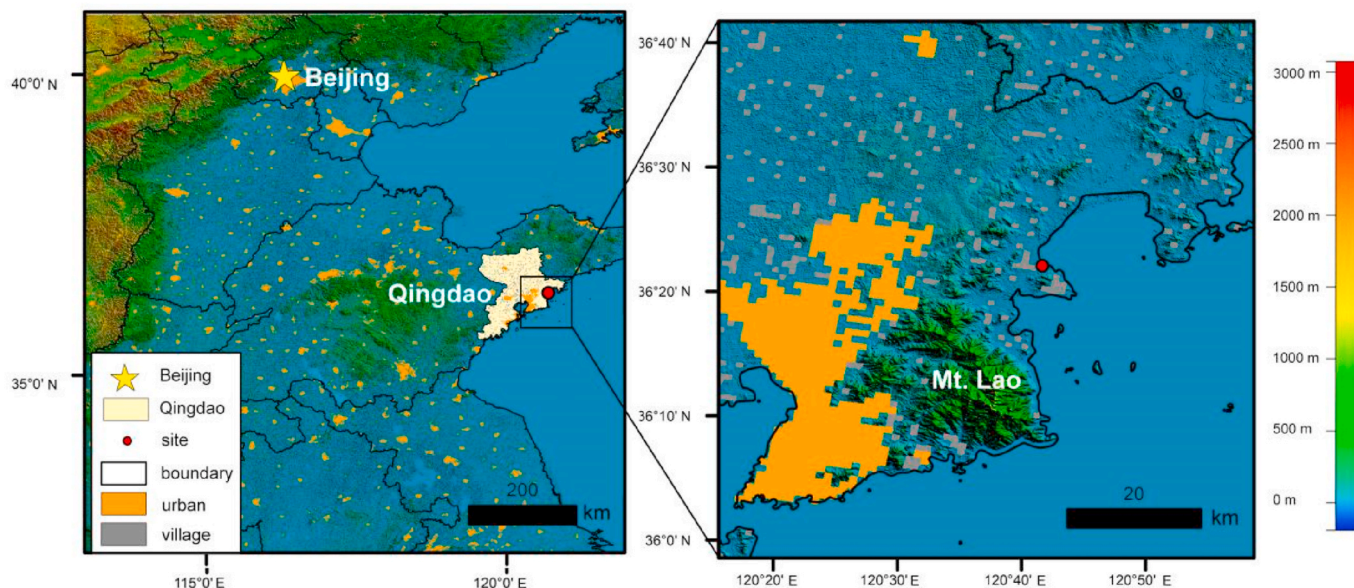

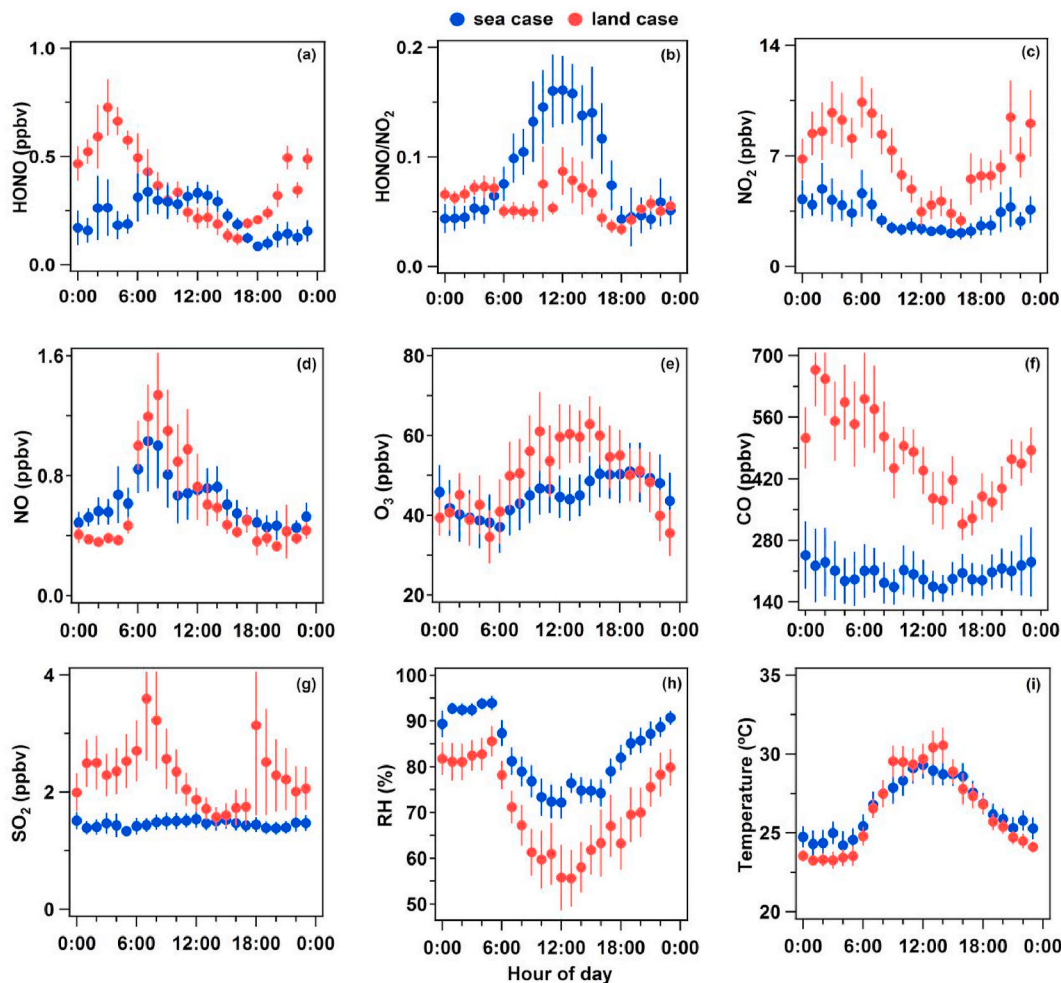**Fig. 1.** Maps showing the location of the measurement site.

Fig. 2. Diurnal variations of HONO, HONO/NO$_2$, and other measured parameters in the "sea case" and the "land case" during the observation. Error bar indicated the standard deviation.

(1) only the nighttime data were selected (from 18:00 to 6:00 in the next morning); (2) the HONO concentration and the ratio of HONO/NO$_2$ continuously increased; (3) wind directions were stable; (4) the concentration of CO was stable; (5) the concentration of NO was low. The criterion (2) and (5) ensure that the increase of HONO concentration is due to the heterogeneous conversion of NO$_2$, and the criterion (3) and (4) further eliminate the influence of suddenly changing air mass. Eight cases were selected according to the above five criteria, including five "sea case" and three "land case" (Fig. S5). Using the cases selected by the above criteria to calculate NO$_2$ to HONO conversion rate could exclude the influence of other chemical or physical processes, and better represent the contribution of heterogeneous conversion of NO$_2$ to HONO formation.

$$C_{HONO} = ([HONO(t_2)] / [NO_2(t_2)] - [HONO(t_1)] / [NO_2(t_1)]) / (t_2 - t_1) \quad (E1)$$

Table 1 summarizes the calculated C$_{HONO}$ and related parameters of the selected eight cases. The C$_{HONO}$ in the "sea case" was significantly higher than that in the "land case", with an average value of 0.045 ± 0.014 h^{-1} and 0.012 ± 0.007 h^{-1}, respectively. The larger nocturnal C$_{HONO}$ in the coastal or marine atmosphere have been reported in several previous studies. For example, Zha et al. (2014) reported C$_{HONO}$ values of (3.17–3.36) × 10^{-2} h^{-1} in air masses passing over sea surface in contrast to values of (1.20–1.30) × 10^{-2} h^{-1} in their "land case". Table S4 summaries the C$_{HONO}$ derived from various urban, rural and coastal environments, and it can be clearly found that C$_{HONO}$ varies greatly in different environments, ranging from 0.0052 h^{-1} to 0.045 h^{-1} (Alicke et al., 2002; Cui et al., 2019; Li et al., 2012, 2018; Su et al.,

Table 1
The nocturnal NO$_2$-to-HONO conversion rates (C$_{HONO}$) and related parameters for the selected "sea case" and "land case".

type	Date	duration (h)	ΔHONO (ppbv)	$\Delta\frac{HONO}{NO_2}$	T (°C)	RH (%)	WS (m s^{-1})	C$_{HONO}$ (h^{-1})
Sea case	23 July	1.13	0.119	0.073	25.2	93.5	1.6	0.0634
	27 July	1.67	0.170	0.049	27.0	94.9	1.0	0.0295
	28 July	0.67	0.131	0.035	28.0	86.5	1.1	0.0529
	2 August	1.83	0.269	0.061	26.0	96.8	2.2	0.0326
	3 August	1.83	0.137	0.088	25.6	95.6	2.3	0.0483
Land case	14 August	0.97	0.133	0.013	23.7	93.8	1.0	0.0130
	14–15 August	5.58	0.204	0.023	23.3	88.9	2.1	0.0041
	16 August	1.97	0.466	0.037	25.9	59.7	0.9	0.0188

2008b; Wang et al., 2013; Wen et al., 2019; Zha et al., 2014). However, it is usually higher in coastal atmosphere impacted by maritime air masses than that in urban (Guangzhou: 0.016 h^{-1}, Kathmandu: 0.014 h^{-1}, Xi'an: 0.0091 h^{-1}, Shanghai: 0.007 h^{-1}) or rural areas (Back garden: 0.024 h^{-1}, Pabstthum: 0.018 h^{-1}, Xin ken: 0.014 h^{-1}).

The strong positive correlation between HONO and NO$_2$ (r = 0.93, Fig. S6a) in these five "sea case" indicated that the strong nocturnal HONO production in maritime air masses was most likely due to heterogeneous conversion of NO$_2$ on/in certain surfaces. The significant difference of C$_{HONO}$ between the "sea case" and the "land case" indicated that soil surface could not be the main reason, because there is no obvious difference in the soil around the measurement site whether towards the sea or the land. The close distance of the measurement site to the sea further excludes this possibility. Another possible surface is the surface of particulate matter. However, the average concentrations of PM$_{2.5}$ in the five "sea case" and three "land case" were relatively low, and did not show the obvious difference (12.46 μg m^{-3} versus 10.55 μg m^{-3}). The negative correlation between HONO and PM$_{2.5}$ (r = −0.26, Fig. S6b) further suggested that primary heterogeneous conversion of NO$_2$ in maritime air masses would not occur on the surface of PM$_{2.5}$. The biggest difference of air masses in the "sea case" and the "land case" is that air masses in the "sea case" spent most of the time passing over the sea. The vast sea surface, especially the surface microlayer, may also be an important medium for heterogeneous conversion of NO$_2$. Previous studies have found that the wet surface can enhance the heterogeneous conversion of NO$_2$ to HONO (Finlayson-Pitts et al., 2003). The sea surface microlayer is an ideal interface, with enough surface water, for this heterogeneous conversion. The strong positive correlation between HONO and temperature (r = 0.79, Fig. S6c), which are also observed by Wojtal et al. (2011) and Wen et al. (2019), is likely an evidence for the production of HONO from the heterogeneous reaction of NO$_2$ on the sea surface microlayer. However, more evidence is needed to further confirm this inference.

3.3. Large daytime unknown HONO source

As mentioned in section 3.1, daytime HONO concentrations can maintain persistently high levels during the daytime in the "sea case", up to 0.3 ppbv even at noon, in contrast to the continuously decreasing concentration in the "land case". Considering that HONO is removed rapidly by photolysis, there must be a strong daytime source related to maritime air masses. To explore the unknown source in the "sea case", the HONO budget was calculated by Equation (2):

2004). The dry deposition velocity of HONO was assumed to be 2.0 cm s^{-1} for both the "sea case" and the "land case" (Harrison et al., 1996), and H was calculated on European Centre for Medium-Range Weather Forecasts website (https://apps.ecmwf.int/datasets/data/interim-full-daily/levtype=sfc/). The OH concentration was obtained from the OBM-AOCP model (Section 2.4), and provided in Fig. S8.

Fig. 3 shows the calculated HONO budget in the "sea case" and the "land case". The maximum value of P$_{other}$ in the "land case" appeared at 10:00, which was consistent with previous observations in inland areas (Huang et al., 2017; Yang et al., 2014). However, the largest value of P$_{other}$ in the "sea case" appeared at noon (11:00–13:00), up to 1.83 ppbv h^{-1}, which was about 61% larger than that in the "land case" (1.14 ppbv h^{-1}). This suggested that there was a strong production of HONO related to maritime air masses during the daytime, which maintained persistently high HONO concentrations even with a rapid photolysis removal.

The correlation analyses of P$_{other}$ in the "sea case" and the "land case" were provided in Fig. 4 and Fig. S7, respectively. In the "land case", the correlation between P$_{other}$ and NO$_2$ was strong (r = 0.62) (Fig. S7), indicating that NO$_2$ conversion may be an important pathway of HONO formation in the "land case". This is consistent with some observations in inland areas (Li et al., 2018; Su et al., 2008b; Huang et al., 2017). However, the correlation between P$_{other}$ and NO$_2$ was weak (r = 0.16) in "sea case" (Fig. 4a), indicating that the heterogeneous conversion of NO$_2$ may not be the main source. As stated in the analysis of nocturnal HONO source, soil cannot be the strong daytime HONO source. The negative correlations of P$_{other}$ and RH (Fig. 4b) also implied that the soil may not contribute to the observed large unknown HONO source, because many previous studies have pointed that soil emissions of HONO were enhanced under high RH conditions (Meusel et al., 2016). Fig. 4c shows that the strength of this unknown source was very consistent with the strength of solar radiation (r = 0.68 for P$_{other}$ and J$_{NO2}$). This suggested that the unknown HONO source should be a photo-enhanced process. Because of the lack of nitrate data, J$_{NO2}$ × PM$_{2.5}$ was used to represent the photolysis of particulate nitrate. Although P$_{other}$ has a good correlation with J$_{NO2}$ × PM$_{2.5}$, its correlation coefficient is significantly lower than that of P$_{other}$ and J$_{NO2}$ (0.68 versus 0.47). The possible contribution of the photolysis of particulate nitrate was further calculated by Equation (3):

$$S_{photo_{NO_3^-}} = [NO_3^-] \times J_{[NO_3^-]} \tag{E3}$$

where [NO$_3^-$] is mass concentration of particulate nitrate, and J$_{[NO3]}$ is the photolysis rate of nitrate. More detailed calculation can be found in the supporting information. The calculated result further indicated that

$$P_{other} = d[HONO] / dt + J_{HONO} \times [HONO] + k_{OH+HONO} \times [HONO] \times [OH] + [HONO] \times v / H - k_{OH+NO} \times [OH] \times [NO] \tag{E2}$$

where, d [HONO]/dt represents the rate of change in the observed HONO concentration, and it can also be expressed as Δ[HONO]/Δt; J$_{HONO}$ × [HONO] represents the loss rate of HONO by photolysis, and J$_{HONO}$ is the photolysis frequency of HONO; k$_{OH+HONO}$ × [OH] × [HONO] represents the gas-phase sink of HONO against OH, and k$_{OH+HONO}$ is the rate constant of HONO with OH; [HONO] × v/H represents dry deposition of HONO, v is dry deposition velocity of HONO, and H is the boundary layer height; k$_{OH+NO}$ × [OH] × [NO] represents gas-phase formation of HONO under photostationary state. The direct emission and vertical transport of HONO were neglected due to its minor contributions compared with other factors at this coastal site (Dillon et al., 2002; Sörgel et al., 2011). We chose 10 min as the time interval for the calculation of HONO budget. J$_{HONO}$ was obtained by the TUV model, and values of 6.0 × 10^{-12} cm^3 molecules^{-1} s^{-1} for k$_{OH+HONO}$ and 9.8 × 10^{-12} cm^3 molecules^{-1} s^{-1} for k$_{OH+NO}$ were adopted (Atkinson et al.,

the photolysis of particulate nitrate may not be an important source of HONO in the marine atmosphere at this coastal site.

We calculated the required HONO flux from the sea to the air to maintain the measured HONO concentration, the detailed calculation was provided in the supporting information. The calculated HONO flux is higher than that measured over the continent (Zhang et al., 2012; Zhou et al., 2001). One possible large daytime HONO source in maritime air masses is the photolysis of nitrogen-containing inorganic or organic compounds on/in the sea surface microlayer. There are abundant nitrate or nitrogen-containing organic compounds in the ocean, especially in the coastal areas (Li et al., 2019; Lam et al., 2011). Due to the alkaline nature of the bulk ocean and the large water solubility of HONO, it should not escape from the bulk ocean into the atmosphere. Therefore, the oceans are previously considered as sinks of HONO. However, the properties of sea surface microlayer were totally different from the bulk
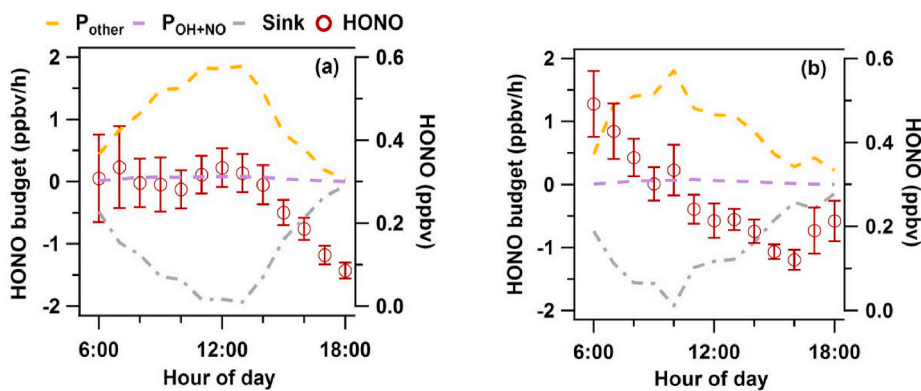
Fig. 3. Daytime HONO budget of the "sea case" (a) and the "land case" (b). Sink $= L_{deposition} + L_{photolysis} + L_{OH+HONO}$. Error bar indicated the standard deviation.
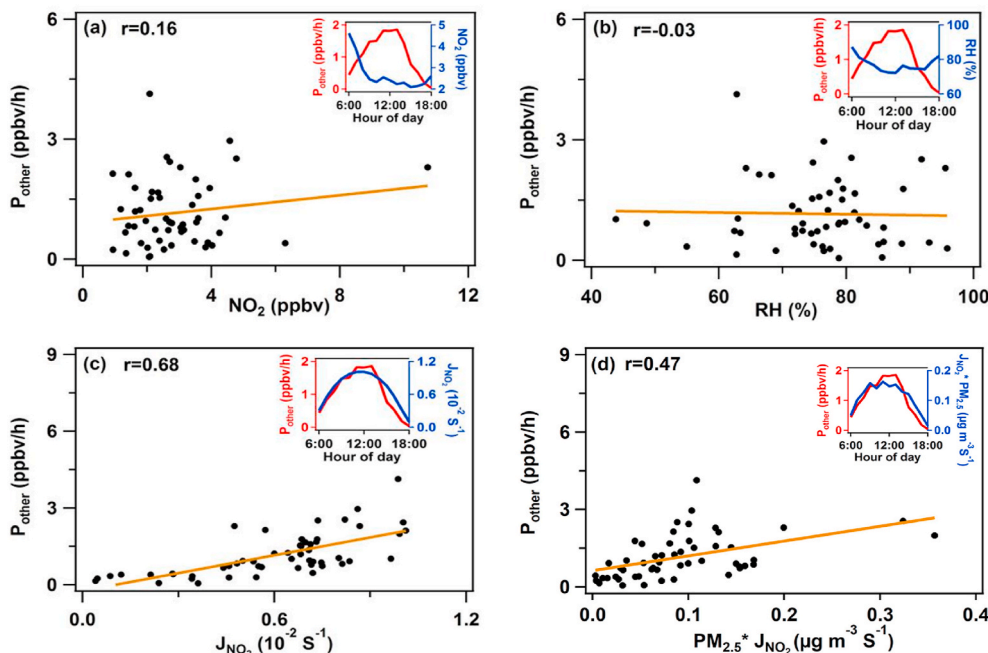

Fig. 4. Correlations of P_{other} with NO_2, RH, J_{NO2}, and $PM_{2.5} \times J_{NO2}$ in the "sea case". The insets show the diurnal variations of P_{other} and NO_2, RH, J_{NO2}, and $PM_{2.5} \times J_{NO2}$.

ocean (Stemmler et al., 2006, 2007). Recent studies have found that even small organic acids with strong acidity such as formic acid could be produced from the heterogeneous reaction on/in the sea surface microlayer and enter into the atmosphere (Mungall et al., 2017). Therefore, the observed strong marine-derived HONO was most likely produced through a photo-enhanced process such as heterogeneous photolysis on/in the sea surface microlayer.

3.4. Impacts on OH and O₃ production

The detailed RO_x radical budget during the observation was explored by the OBM-AOCP model. Fig. 5 shows the diurnal variations of primary sources production rates of OH, RO_2, and HO_2 radicals in the "sea case" (Fig. 5a–c) and the "land case" (Fig. 5d–f). For primary OH production, HONO photolysis is the predominant source in the "sea case" not only in the early morning but throughout the daytime, contributing to an average production rate of 0.49 ppbv h^{-1}, which was 1.3 times higher than that from photolysis of O₃ (0.38 ppbv h^{-1}). The contributions of HONO photolysis were up to 1.30 ppbv h^{-1} at noon in the "sea case", which was 2 times higher than that in the "land case" (0.66 ppbv h^{-1}). In addition, ozonolysis reactions of unsaturated VOCs in the "sea case" and

the "land case" are another considerable OH source with an average production rate of 0.04 ppbv h^{-1} and 0.06 ppbv h^{-1}, respectively, while other sources (e.g., photolysis of HNO_3 and OVOCs) are negligible.

For RO_2 radical, the most important source was OVOCs photolysis in both the "sea case" and the "land case", with the same average production rate of 0.15 ppbv h^{-1}, followed by the NO_3 oxidation of VOCs (0.06 ppbv h^{-1} in the "sea case", and 0.12 ppbv h^{-1} in the "land case"). Furthermore, the production rate of ozonolysis reactions of VOCs for RO_2 radical was also worth noting (0.04 ppbv h^{-1} in the "sea case", and 0.06 ppbv h^{-1} in the "land case"). For HO_2 radical, the HCHO photolysis was the main source with an average production rate of 0.22 ppbv h^{-1} in the "sea case" and 0.30 ppbv h^{-1} in the "land case". Photolysis of other OVOCs was the second-most important source of HO_2 with an average production rate of 0.11 ppbv h^{-1} in the "sea case" and 0.12 ppbv h^{-1} in the "land case", respectively.

Fig. 6 shows the average diurnal variations of the production rate of OH and O₃ in the "sea case" and the "land case" modelled with/without the constraints of measured HONO. In terms of the entire daytime, the average OH production rates in the "sea case" and the "land case" were 0.94 ppbv h^{-1} and 1.02 ppbv h^{-1}, respectively, when only considering gas-phase reaction of OH and NO. When the measured HONO was input
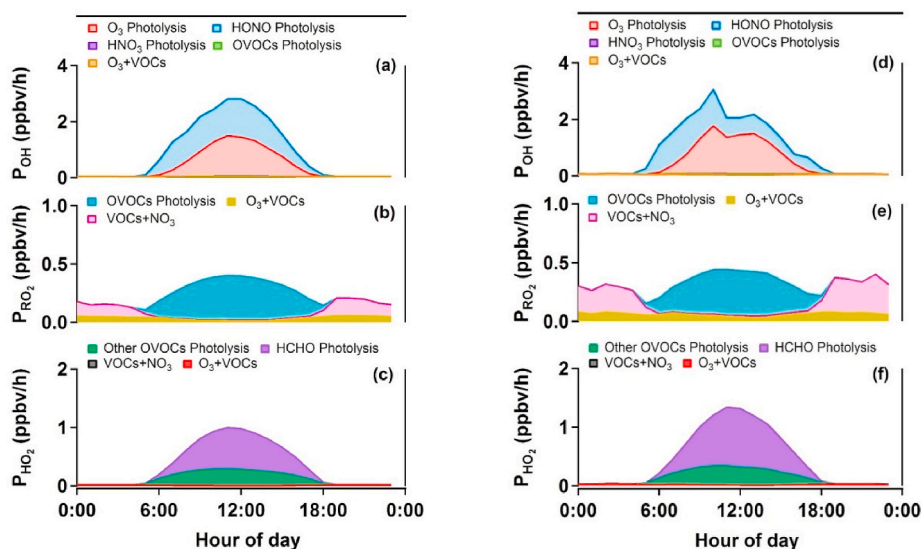
Fig. 5. Model-simulated average diurnal variations of primary sources of OH, RO_2, and HO_2 in the "sea case" (a, b, and c) and the "land case" (d, e, and f).
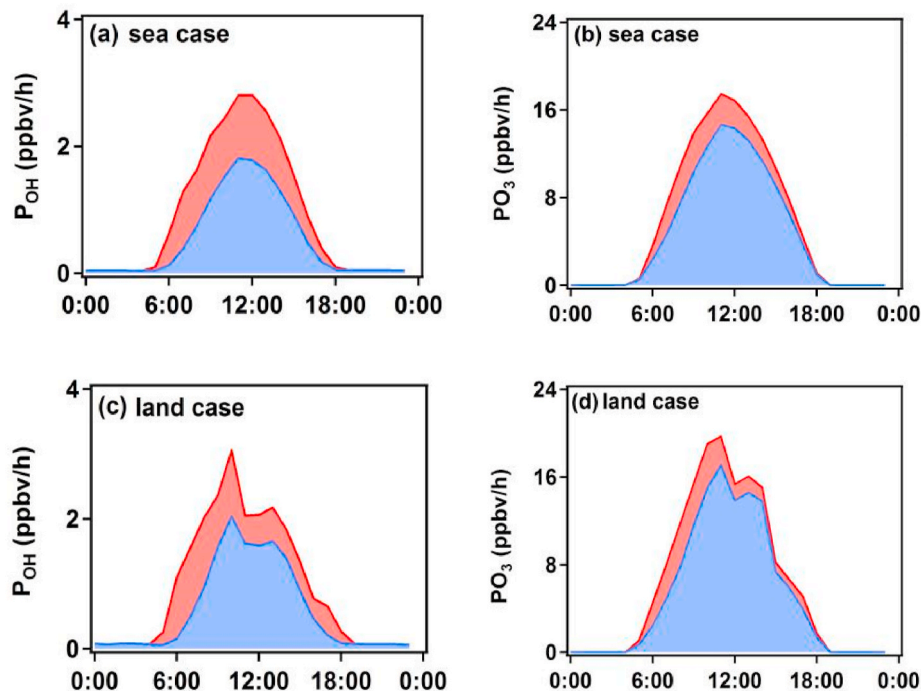

Fig. 6. Model-simulated average diurnal variations of production rate of OH and O_3 in the "sea case" (a, b) and the "land case" (c, d), with (red) and without (blue) the constraints of measured HONO. (For interpretation of the references to colour in this figure legend, the reader is referred to the Web version of this article.)

in the model, the average OH production rate increased by 76% (1.65 ppbv h^{-1}) and 61% (1.64 ppbv h^{-1}) in the "sea case" and the "land case", respectively. The average O_3 production rates in the "sea case" and the "land case" were 8.61 ppbv h^{-1} and 9.22 ppbv h^{-1}, respectively, without the constraints of measured HONO, and increased by 24% (10.66 ppbv h^{-1}) and 22% (11.29 ppbv h^{-1}) when the measured HONO was input. Overall, the marine-derived HONO contributed significantly to OH and O_3 production, which was comparable to or larger than that in the "land case". This indicates that the HONO in the marine atmosphere plays a vital role in the atmospheric chemistry, and more studies are required to explore its detailed formation mechanisms.

4. Conclusions

In this study, we distinguished HONO production in the "sea case" and the "land case" by wind direction and backward air mass trajectory in a field observation conducted at a coastal site in Qingdao, China, in the summer of 2019. Quite different diurnal variations of HONO were observed in the "sea case", with persistently high concentrations during the daytime, in contrast to the continuously decreasing concentrations in the "land case". Both the much larger nocturnal NO_2-to-HONO conversion rate and the daytime P_{other} in the "sea case" suggested that strong marine-derived HONO production may have been overlooked so far. Correlation analysis implied that sea surface microlayer is likely to be a media for the formation of HONO through the heterogeneous conversion of NO_2 and photolysis of nitrogen-containing compounds in

the nocturnal and daytime, respectively. These marine-derived HONO contributed significantly to the production of both OH and O_3. More research is needed to confirm the sources of HONO in the marine atmosphere to better understand its contributions to OH and O_3 production.

CRediT authorship contribution statement

Juan Yang: Conceptualization, Formal analysis, Writing - original draft. **Hengqing Shen:** Conceptualization, Supervision, Writing - review & editing. **Ming-Zhi Guo:** Supervision, Writing - review & editing. **Min Zhao:** Visualization, Methodology. **Ying Jiang:** Investigation, Data curation. **Tianshu Chen:** Investigation, Visualization. **Yuhong Liu:** Investigation. **Hongyong Li:** Investigation. **Yujiao Zhu:** Resources, Funding acquisition. **He Meng:** Resources. **Wenxing Wang:** Supervision, Resources. **Likun Xue:** Conceptualization, Funding acquisition, Project administration, Writing - review & editing.

Declaration of competing interest

The authors declare that they have no known competing financial interests or personal relationships that could have appeared to influence the work reported in this paper.

Acknowledgements

Appendix A. Supplementary data

Supplementary data to this article can be found online at https://doi.org/10.1016/j.atmosenv.2020.117948.

References

Acker, K., Möller, D., Wieprecht, W., Meixner, F.X., Bohn, B., Gilge, S., Plass-Dülmer, C., Berresheim, H., 2006. Strong daytime production of OH from HNO_2 at a rural mountain site. Geophys. Res. Lett. 33, L02809. https://doi.org/10.1029/2005gl024643.

Alicke, B., Platt, U., Stutz, J., 2002. Impact of nitrous acid photolysis on the total hydroxyl radical budget during the Limitation of Oxidant Production/Pianura Padana Produzione di Ozono study in Milan. J. Geophys. Res. 107, 8196. https://doi.org/10.1029/2000jd000075.

Amoroso, A., Beine, H.J., Esposito, G., Perrino, C., Catrambone, M., Allegrini, I., 2007. Seasonal differences in atmospheric nitrous acid near mediterranean urban areas. Water, Air, Soil Pollut. 188, 81–92. https://doi.org/10.1007/s11270-007-9526-6.

Atkinson, R., Baulch, D.L., Cox, R.A., Crowley, J.N., Hampson, R.F., Hynes, R.G., Jenkin, M.E., Rossi, M.J., Troe, J., 2004. Evaluated kinetic and photochemical data for atmospheric chemistry: Part 1-gas phase reactions of O_x, HO_x, NO_x and SO_x species. Atmos. Chem. Phys. 4, 1461–1738. https://doi.org/10.5194/acp-4-1461-2004.

Bernard, F.O., Cazaunau, M., Grosselin, B.t., Zhou, B., Zheng, J., Liang, P., Zhang, Y., Ye, X., Daële, V., Mu, Y., 2015. Measurements of nitrous acid (HONO) in urban area of Shanghai, China. Environ. Sci. Pollut. Control Ser. 23, 5818–5829. https://doi.org/10.1007/s11356-015-5797-4.

Benedict, K.B., McFall, A.S., Anastasio, C., 2017. Quantum yield of nitrite from the photolysis of aqueous nitrate above 300 nm. Environ. Sci. Technol. 51, 4387–4395. https://doi.org/10.1021/acs.est.6b06370.

Cui, L., Li, R., Fu, H., Li, Q., Zhang, L., George, C., Chen, J., 2019. Formation features of nitrous acid in the offshore area of the East China Sea. Sci. Total Environ. 682, 138–150. https://doi.org/10.1016/j.scitotenv.2019.05.004.

Dillon, M.B., Lamanna, M.S., Schade, G.W., Goldstein, A., Cohen, R.C., 2002. Chemical evolution of the Sacramento urban plume: transport and oxidation. J. Geophys. Res. 107, 4045. https://doi.org/10.1029/2001JD000969.

Finlayson-Pitts, B.J., Wingen, L.M., Sumner, A.L., Syomin, D., Ramazan, K.A., 2003. The heterogeneous hydrolysis of NO_2 in laboratory systems and in outdoor and indoor

atmospheres: an integrated mechanism. Phys. Chem. Chem. Phys. 5, 223–242. https://doi.org/10.1039/B208564J.

Gu, R., Zheng, P., Chen, T., Dong, C., Wang, Y., Liu, Y., Liu, Y., Luo, Y., Han, G., Wang, X., Zhou, X., Wang, T., Wang, W., Xue, L., 2020. Atmospheric nitrous acid (HONO) at a rural coastal site in North China: seasonal variations and effects of biomass burning. Atmos. Environ. 229, 117429. https://doi.org/10.1016/j.atmosenv.2020.117429.

Harrison, R.M., Peak, J.D., Collins, G.M., 1996. Tropospheric cycle of nitrous acid. J. Geophys. Res.: Atmospheres 101, 14429–14439. https://doi.org/10.1029/96JD00341.

Huang, R., Yang, L., Cao, J., Wang, Q., Tie, X., Ho, Kin-Fai, Shen, Z., Zhang, R., Li, G., Zhu, C., Zhang, N., Dai, W., Zhou, J., Liu, S., Chen, Y., Chen, J., Colin, D.O., 2017. Concentration and sources of atmospheric nitrous acid (HONO) at an urban site in Western China. Sci. Total Environ. 593, 165–172. https://doi.org/10.1016/j.scitotenv.2017.02.166.

Kleffmann, J., Gavriloaiei, T., Hofzumahaus, A., Holland, F., Koppmann, R., Rupp, L., Schlosser, E., Siese, M., Wahner, A., 2005. Daytime formation of nitrous acid: a major source of OH radicals in a forest. Geophys. Res. Lett. 32 https://doi.org/10.1029/2005gl022524.

Kurtenbach, R., Becker, K.H., Gomes, J.A.G., Kleffmann, J., Lorzer, J.C., Spittler, M., Wiesen, P., Ackermann, R., Geyer, A., Platt, U., 2001. Investigations of emissions and heterogeneous formation of HONO in a road traffic tunnel. Atmos. Environ. 35, 3385–3394. https://doi.org/10.1016/S1352-2310(01)00138-8.

Lee, J.D., Whalley, L.K., Heard, D.E., Stone, D., Dunmore, R.E., Hamilton, J.F., et al., 2016. Detailed budget analysis of HONO in central London reveals a missing daytime source. Atmos. Chem. Phys. 16, 2747–2764. https://doi.org/10.5194/acp-16-2747-2016.

Li, Z., Li, M., Wang, C., Zhou, X., Li, J., Li, D., 2019. Highly sensitive and selective method for detection of trace amounts of nitrite in aquaculture water by SERRS coupled with diazo reaction. Sensor. Actuator. B Chem. 297, 126757. https://doi.org/10.1016/j.snb.2019.126757.

Li, D.D., Xue, L.K., Wen, L., Wang, X.F., Chen, T.S., Mellouki, A., et al., 2018. Characteristics and sources of nitrous acid in an urban atmosphere of northern China: results from 1-yr continuous observations. Atmos. Environ. 182, 296–306. https://doi.org/10.1016/j.atmosenv.2018.03.033.

Li, X., Brauers, T., Häseler, R., Bohn, B., Fuchs, H., Hofzumahaus, A., Holland, F., Lou, S., Lu, K.D., Rohrer, F., Hu, M., Zeng, L.M., Zhang, Y.H., Garland, R.M., Su, H., Nowak, A., Wiedensohler, A., Takegawa, N., Shao, M., Wahner, A., 2012. Exploring the atmospheric chemistry of nitrous acid (HONO) at a rural site in Southern China. Atmos. Chem. Phys. 12, 1497–1513. https://doi.org/10.5194/acp-12-1497-2012.

Lam, P., Jensen, M.M., Kock, A., Lettmann, K.A., Plancherel, Y., Lavik, G., Bange, H.W., Kuypers, M.M.M., 2011. Origin and fate of the secondary nitrite maximum in the Arabian Sea. Biogeosciences 8, 1565–1577. https://doi.org/10.5194/bg-8-1565-2011.

Meusel, H., Kuhn, U., Reiffs, A., Mallik, C., Harder, H., Martinez, M., et al., 2016. Daytime formation of nitrous acid at a coastal remote site in Cyprus indicating a common ground source of atmospheric HONO and NO. Atmos. Chem. Phys. 16, 14475–14493. https://doi.org/10.5194/acp-16-14475-2016.

Michoud, V., Colomb, A., Borbon, A., Miet, K., Beekmann, M., Camredon, M., et al., 2014. Study of the unknown HONO daytime source at a European suburban site during the MEGAPOLI summer and winter field campaigns. Atmos. Chem. Phys. 14, 2805–2822. https://doi.org/10.5194/acp-14-2805-2014.

Mungall, E.L., Abbatt, J.P.D., Wentzell, J.J.B., Lee, A.K.Y., Thomas, J.L., Blais, M., Gosselin, M., Miller, L.A., Papakyriakou, T., Willis, M.D., 2017. Microlayer source of oxygenated volatile organic compounds in the summertime marine Arctic boundary layer. Proc. Natl. Acad. Sci. U.S.A. 114, 6203–6208. https://doi.org/10.1073/pnas.1620571114.

Nie, W., Ding, A.J., Xie, Y.N., Xu, Z., Mao, H., Kerminen, V.-M., Zheng, L.F., Qi, X.M., Huang, X., Yang, X.-Q., Sun, J.N., Herrmann, E., Petäjä, T., Kulmala, M., Fu, C.B., 2015. Influence of biomass burning plumes on HONO chemistry in eastern China. Atmos. Chem. Phys. 15, 1147–1159. https://doi.org/10.5194/acp-15-1147-2015.

Qin, M., Xie, P., Su, H., Gu, J., Peng, F., Li, S., Zeng, L., Liu, J., Liu, W., Zhang, Y., 2009. An observational study of the HONO–NO_2 coupling at an urban site in Guangzhou City, South China. Atmos. Environ. 43, 5731–5742. https://doi.org/10.1016/j.atmosenv.2009.08.017.

Ren, X., Gao, H., Zhou, X., Crounse, J.D., Wennberg, P.O., Browne, E.C., LaFranchi, B.W., Cohen, R.C., McKay, M., Goldstein, A.H., Mao, J., 2010. Measurement of atmospheric nitrous acid at Bodgett Forest during BEARPEX2007. Atmos. Chem. Phys. 10, 6283–6294. https://doi.org/10.5194/acp-10-6283-2010.

Sun, L., Chen, T., Jiang, Y., Zhou, Y., Sheng, L., Lin, J., Li, J., Dong, C., Wang, C., Wang, X., Zhang, Q., Wang, W., Xue, L., 2020. Ship emission of nitrous acid (HONO) and its impacts on the marine atmospheric oxidation chemistry. Sci. Total Environ. 735, 139335. https://doi.org/10.1016/j.scitotenv.2020.139355.

Sörgel, M., Regelin, E., Bozem, H., Diesch, J.M., Drewnick, F., Fischer, H., Harder, H., Held, A., Hosaynali-Beygi, Z., Martinez, M., Zetzsch, C., 2011. Quantification of the unknown HONO daytime source and its relation to NO_2. Atmos. Chem. Phys. 11, 10433–10447. https://doi.org/10.5194/acp-11-10433-2011.

Spataro, F., Ianniello, A., 2014. Sources of atmospheric nitrous acid: state of the science, current research needs, and future prospects. J. Air Waste Manag. Assoc. 64, 1232–1250. https://doi.org/10.1080/10962247.2014.952846.

Spataro, F., Ianniello, A., Esposito, G., Allegrini, I., Zhu, T., Hu, M., 2013. Occurrence of atmospheric nitrous acid in the urban area of Beijing (China). Sci. Total Environ. 447, 210–224. https://doi.org/10.1016/j.scitotenv.2012.12.065.

Stemmler, K., Ammann, M., Donders, C., Kleffmann, J., George, C., 2006. Photosensitized reduction of nitrogen dioxide on humic acid as a source of nitrous acid. Nature 440, 195–198. https://doi.org/10.1038/nature04603.

Stemmler, K., Ndour, M., Elshorbany, Y., Kleffmann, J., D'Anna, B., George, C., Bohn, B., Ammann, M., 2007. Light induced conversion of nitrogen dioxide into nitrous acid on submicron humic acid aerosol. Atmos. Chem. Phys. 7, 4237–4248. https://doi.org/10.5194/acp-7-4237-2007.

Su, H., Cheng, Y., Oswald, R., Behrendt, T., Trebs, I., Meixner, F.X., Andreae, M., Cheng, P., Zhang, Y., Poeschl, U., 2011. Soil nitrite as a source of atmospheric HONO and OH radicals. Science 333, 1616–1618. https://doi.org/10.1126/science.1207687.

Su, H., Cheng, Y.F., Cheng, P., Zhang, Y.H., Dong, S., Zeng, L.M., Wang, X., Slanina, J., Shao, M., Wiedensohler, A., 2008a. Observation of nighttime nitrous acid (HONO) formation at a non-urban site during PRIDE-PRD 2004 in China. Atmos. Environ. 42, 6219–6232. https://doi.org/10.1016/j.atmosenv.2008.04.006.

Su, H., Cheng, Y.F., Shao, M., Gao, D.F., Yu, Z.Y., Zeng, L.M., Slanina, J., Zhang, Y.H., Wiedensohler, A., 2008b. Nitrous acid (HONO) and its daytime sources at a rural site during the 2004 PRIDE-PRD experiment in China. J. Geophys. Res. 113, D14312 https://doi.org/10.1029/2007jd009060.

Tong, S., Hou, S., Zhang, Y., Chu, B., Liu, Y., He, H., Zhao, P., Ge, M., 2015. Comparisons of measured nitrous acid (HONO) concentrations in a pollution period at urban and suburban Beijing, in autumn of 2014. Sci. China Chem. 58, 1393–1402. https://doi.org/10.1007/s11426-015-5454-2.

Tsai, C., Spolaor, M., Colosimo, S.F., Pikelnaya, O., Stutz, J., 2018. Nitrous acid formation in a snow-free wintertime polluted rural area. Atmos. Chem. Phys. 18, 1977–1996. https://doi.org/10.5194/acp-18-1977-2018.

VandenBoer, T.C., Brown, S.S., Murphy, J.G., Keene, W.C., Young, C.J., Pszenny, A.A.P., Kim, S., Warneke, C., de Gouw, J.A., Maben, J.R., Wagner, N.L., Riedel, T.P., Thornton, J.A., Wolfe, D.E., Dube, W.P., Ozturk, F., Brock, C.A., Grossberg, N., Lefer, B., Lerner, B., Middlebrook, A.M., Roberts, J.M., 2014. Understanding the role of the ground surface in HONO vertical structure: high resolution vertical profiles during NACHTT-11. J. Geophys. Res.: Atmospheres 118, 10155–10171. https://doi.org/10.1002/jgrd.50721.

Villena, G., Wiesen, P., Cantrell, C.A., Flocke, F., Fried, A., Hall, S.R., et al., 2011. Nitrous acid (HONO) during polar spring in Barrow, Alaska: a net source of OH radicals? J. Geophys. Res. 116, D00R07 https://doi.org/10.1029/2011jd016643.

Wang, S., Zhou, R., Zhao, H., Wang, Z., Chen, L., Zhou, B., 2013. Long-term observation of atmospheric nitrous acid (HONO) and its implication to local NO_2 levels in Shanghai, China. Atmos. Environ. 77, 718–724. https://doi.org/10.1016/j.atmosenv.2013.05.071.

Wang, X., Wang, W., Yang, L., Gao, X., Wei, N., Yu, Y., Xu, P., Yang, Z., Wang, Z., 2012. The secondary formation of inorganic aerosols in the droplet mode through heterogeneous aqueous reactions under haze conditions. Atmos. Environ. 63, 68–76. https://doi.org/10.1016/j.atmosenv.2012.09.029.

Wen, L., Chen, T., Zheng, P., Wu, L., Wang, X., Mellouki, A., Xue, L., Wang, W., 2019. Nitrous acid in marine boundary layer over eastern Bohai Sea, China: characteristics, sources, and implications. Sci. Total Environ. 670, 282–291. https://doi.org/10.1016/j.scitotenv.2019.03.225.

Wojtal, P., Halla, J.D., McLaren, R., 2011. Pseudo steady states of HONO measured in the nocturnal marine boundary layer: a conceptual model for HONO formation on aqueous surfaces. Atmos. Chem. Phys. 11, 3243–3261. https://doi.org/10.5194/acp-11-3243-2011.

Xue, L., Gu, R., Wang, T., Wang, X., Saunders, S., Blake, D., Louie, P.K.K., Luk, C.W.Y., Simpson, I., Xu, Z., Wang, Z., Gao, Y., Lee, S., Mellouki, A., Wang, W., 2016. Oxidative capacity and radical chemistry in the polluted atmosphere of Hong Kong and Pearl River Delta region: analysis of a severe photochemical smog episode. Atmos. Chem. Phys. 16, 9891–9903. https://doi.org/10.5194/acp-16-9891-2016.

Xue, L., Wang, T., Gao, J., Ding, A.J., Zhou, X.H., Blake, D.R., et al., 2014. Ground-level ozone in four Chinese cities: precursors, regional transport and heterogeneous processes. Atmos. Chem. Phys. 14, 13175–13188. https://doi.org/10.5194/acp-14-13175-2014.

Yang, Q., Su, H., Li, X., Cheng, Y.F., Lu, K.D., Cheng, P., Gu, J.W., Guo, S., Hu, M., Zeng, L.M., Zhu, T., Zhang, Y.H., 2014. Daytime HONO formation in the suburban area of the megacity Beijing, China. Sci. China Chem. 57, 1032–1042. https://doi.org/10.1007/s11426-013-5044-0.

Ye, C., Zhou, X., Dennis, P., Jochen, S., James, F., Max, S., Catalina, T., Christopher, C.R. L., Mauldin, I.I.I., Teresa, C., Andrew, W., Rebecca, S.H., Eric, C.A., Alex, G., Lisa, K., Yuan, B., Thomas, K., Julie, H., Samuel, H., Kirk, U., James, N.S., John, O., Christoph, K., 2016. Rapid cycling of reactive nitrogen in the marine boundary layer. Nature 532, 489–491. https://doi.org/10.1038/nature17195.

Zha, Q., Xue, L., Wang, T., Xu, Z., Yeung, C., Louie, P.K.K., Luk, C.W.Y., 2014. Large conversion rates of NO_2 to HNO_2 observed in air masses from the South China Sea: evidence of strong production at sea surface? Geophys. Res. Lett. 41, 7710–7715. https://doi.org/10.1002/2014gl061429.

Zhang, N., Zhou, X., Shepson, Paul B., Gao, H.L., Alaghmand, M., Stirm, B., 2009. Aircraft measurement of HONO vertical profiles over a forested region. Geophys. Res. Lett. 36, L15820 https://doi.org/10.1029/2009gl038999.

Zhang, N., Zhou, X., Bertman, S., Tang, D., Alaghmand, M., Shepson, P.B., Carroll, M.A., 2012. Measurements of ambient HONO concentrations and vertical HONO flux above a northern Michigan forest canopy. Atmos. Chem. Phys. 12, 8285–8296. https://doi.org/10.5194/acp-12-8285-2012.

Zhang, W.Q., Tong, S.R., Ge, M.F., An, J.L., Shi, Z.B., Hou, S.Q., et al., 2018. Variations and sources of nitrous acid (HONO) during a severe pollution episode in Beijing in winter 2016. Sci. Total Environ. 648, 253–262. https://doi.org/10.1016/j.scitotenv.2018.08.133.

Zhou, X., Beine, H.J., Honrath, R.E., Fuentes, J.D., Simpson, W., Shepson, P.B., Bottenheim, J.W., 2001. Snowpack photochemical production of HONO: a major source of OH in the Arctic boundary layer in springtime. Geophys. Res. Lett. 28, 4087–4090. https://doi.org/10.1029/2001gl013531.

Zhou, X., Huang, G., Civerolo, K., Roychowdhury, U., Demerjian, K.L., 2007. Summertime observations of HONO, HCHO, and O_3 at the summit of whiteface mountain, New York. J. Geophys. Res. 112, D08311 https://doi.org/10.1029/2006jd007256.